

# Colloidal Gelation Through Thermally-Triggered Surfactant Displacement

Li-Chiun Cheng, Zachary M. Sherman, James W. Swan and Patrick S. Doyle\*

Department of Chemical Engineering, Massachusetts Institute of Technology, Cambridge, Massachusetts 02139, USA.

\*corresponding email: pdoyle@mit.edu

## S1 Nanoemulsion synthesis and stability

### S1.1 Control of nanoemulsion droplet size

The nanoemulsions were made using high pressure homogenization, which allows easy preparation of large quantities of emulsions with a range of droplet sizes.<sup>1</sup> In this work, the nanoemulsion droplet diameter ( $D$ ) was controlled by the number of homogenizing passes ( $N$ ) at a fixed homogenizing pressure  $\Delta P = 18$  kpsi. Nanoemulsions discussed here consist of PDMS droplets (volume fraction  $\phi = 0.30$ ) dispersed in an aqueous continuous phase containing PEGMA (volume fraction  $P = 0.33$ ) and SDS with a total concentration = 175 mM in the system. The droplet size was determined using dynamic light scattering after diluting the nanoemulsion to  $\phi = 0.002$  using an aqueous diluting agent with  $P = 0.33$  (Methods).

To synthesize the nanoemulsion, a pre-emulsion was first obtained by adding PDMS into a pre-mix aqueous continuous phase with  $P = 0.33$  and  $[SDS] = 175$  mM, and the mixture was then agitated using magnetic stirring for 15 minutes. The pre-emulsion was processed into the nanoemulsion with high pressure homogenization. Figure S1 shows the droplet size as a function of  $N$  at  $\Delta P = 18$  kpsi. The variation of droplet size follows an empirical exponential decay with  $N$ , as shown by the solid line in Figure S1.<sup>1,2</sup>

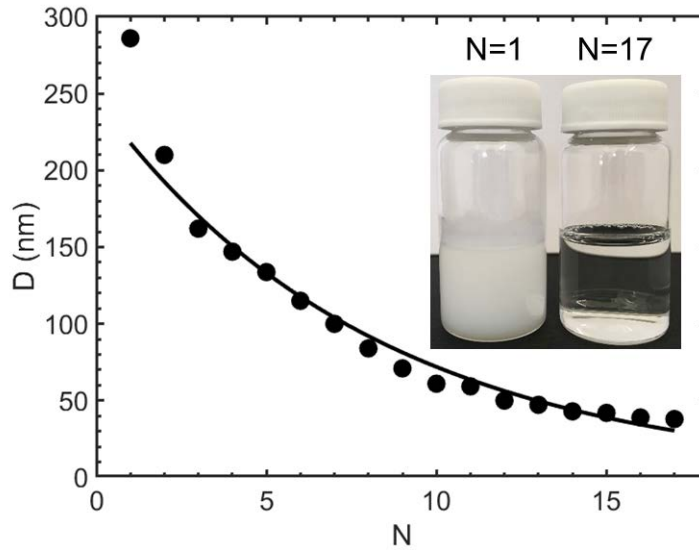


Figure S1. Evolution of nanoemulsion droplet diameter,  $D$ , with the number of homogenization passes,  $N$ . The size variation is fitted with an exponentially-decay function as shows by the solid line. The inset photograph shows the appearance of the nanoemulsion after  $N = 1$  (opaque) and  $N = 17$  (transparent).

### S1.2 Nanoemulsion stability

The droplet stability was tested by investigating the effect of thermal gelation. The experiment was conducted by a series of temperature-jump steps. First, the nanoemulsion ( $P = 0.33$ ,  $\phi = 0.3$  and  $D = 53$  nm) was placed in an oven where the temperature was kept at  $55.0$  °C for 10 minutes. After the gelation is induced (Figure 1b), the nanoemulsion was cooled to  $4$  °C for 15 minute to ensure sufficient cooling. By applying a gentle shear, the nanoemulsion was able to re-enter to liquid-state (see S2 for a more detailed discussion on the recovery of the nanoemulsion system using rheometry). The droplet size was then measured using DLS, and the diameter was only slightly increased to  $D = 55$ nm. Such increase in droplet size might result from 1) the rate of Oswald ripening is increased at elevated temperatures,<sup>1</sup> and 2) the oil/water interface is less stabilized during the surfactant displacement. However, the result still suggests the process of gelation does not significantly (less than 5%) affect the size of the droplets.

Another droplet stability test was also applied to monitor the size of nanoemulsion droplets in the PEGMA solution as a function of temperature using DLS. The data is shown in Figure S2 below. Before each DLS measurement, the nanoemulsion is diluted by a PEGMA aqueous solution ( $P =$

0.33) and the resulting oil volume fraction is 0.1%. As shown, the droplet size stays stable across the experimental temperature window, suggesting PEGMA does not dissolve in the oil droplets.

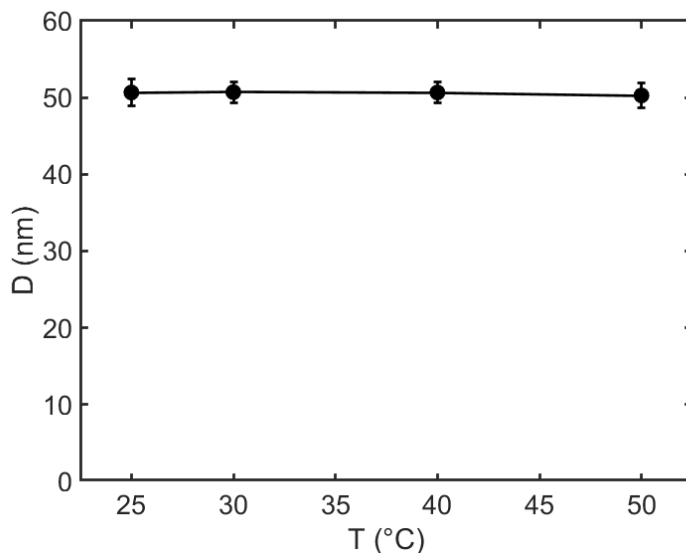


Figure S2. Nanoemulsion droplet size as a function of temperature. The error bars are standard errors from 3-5 independent measurements.

## S2 Rheological characterization of the model nanoemulsion system

### S2.1 Linear viscoelasticity and the plateau modulus of the canonical nanoemulsion

To determine the gelation temperature ( $T_{\text{gel}}$ ) and the plateau modulus ( $G_{\text{p}}$ ) of the nanoemulsion gels, we measured the linear viscoelasticity, storage modulus  $G'(\omega)$  and loss modulus  $G''(\omega)$ , at rising temperatures. The results of the canonical nanoemulsion ( $D = 50$  nm,  $P = 0.33$  and  $\phi = 0.3$ ) are shown in Figure S3a (and Figure 1a). At the room temperature, the nanoemulsion shows a liquid-like behavior. A critical sol-gel transition is found at  $T = 30.0$  °C where  $G'(\omega) \sim G''(\omega) \sim \omega^n$  using the classic Chambon-Winter criterion,<sup>3,4</sup> and a gelation temperature,  $T_{\text{gel}}$ , is determined. As further increasing the temperature,  $G'$  and  $G''$  grow, and  $G'$  becomes nearly independent of the applied frequency. In this high temperature regime, we found that the viscoelastic moduli do not appreciably change when  $T \geq T_{\text{gel}} + 20$  °C (i.e.  $T \geq 50$  °C in Figure S3a). Therefore, in this work we determined the plateau modulus of all nanoemulsions with different formulations at a

temperature of  $T_{\text{gel}} + 25 \text{ }^\circ\text{C}$  (Figure 1a and Figure 4 to 6), and the  $T_{\text{gel}}$  of each sample was determined using the Chambon-Winter criterion.<sup>3,4</sup>

## S2.2 Reversibility and recovery of the nanoemulsion gel

Rheological characterization combining small-amplitude oscillatory shear (SAOS, shear strain equal to 0.05%) and large-amplitude shear (LAOS) at a fixed angular frequency  $\omega = 20 \text{ rad s}^{-1}$  was used to test the reversibility and recovery of the nanoemulsion gel (Figure S3b). The characterization was composed of three steps of time-sweep measurements. First, the linear viscoelasticity was measured using SAOS at  $T = 20 \text{ }^\circ\text{C}$ . As shown, the nanoemulsion showed a liquid-like behavior with  $G'' \gg G'$  over the experimental window. Subsequently, the temperature was raised to  $55 \text{ }^\circ\text{C}$ , and the SAOS measurement started once the system reached the target temperature. The storage and loss moduli reached a plateau after  $\approx 500$  seconds, and the nanoemulsion showed a solid-like behavior as expected. Finally, the temperature was either decreased to  $20 \text{ }^\circ\text{C}$  or kept at  $55 \text{ }^\circ\text{C}$  in the third step. Once the target temperature was reached, a LAOS with a shear stress,  $\sigma > \sigma_y$  (where  $\sigma_y$  is the yield stress determined in Figure S3c), was applied to the nanoemulsion for 60 seconds, and the SAOS was then performed to measure the linear viscoelasticity.

The reversibility test (20-55-20  $^\circ\text{C}$  route) supports the existence of an energetic barrier in the estimated interactive potential (Figure 2c). When the temperature is decrease from 55 to 20  $^\circ\text{C}$ , the system is still trapped in the energy minimum, and the nanoemulsion still shows significant elasticity over the experimental window (Figure S3b). When larger  $\sigma$  is applied, the system can more easily escape from the energy minimum and re-enter the liquid state, supporting our estimated interactive potentials and the proposed gelling mechanism where the system needs to overcome an energetic barrier to undergo gelation. On the other hand, the recovery test (20-55-55  $^\circ\text{C}$  route) shows that storage and loss moduli decrease after a shear stress is applied. Such decrease is possibly due to a slow structural relaxation that has been found in similar colloidal gel systems<sup>5</sup> when the system is directly quenched to a state far from equilibrium<sup>6</sup>. It has been found that applying a large shear can facilitate such structural relaxation<sup>5</sup>.

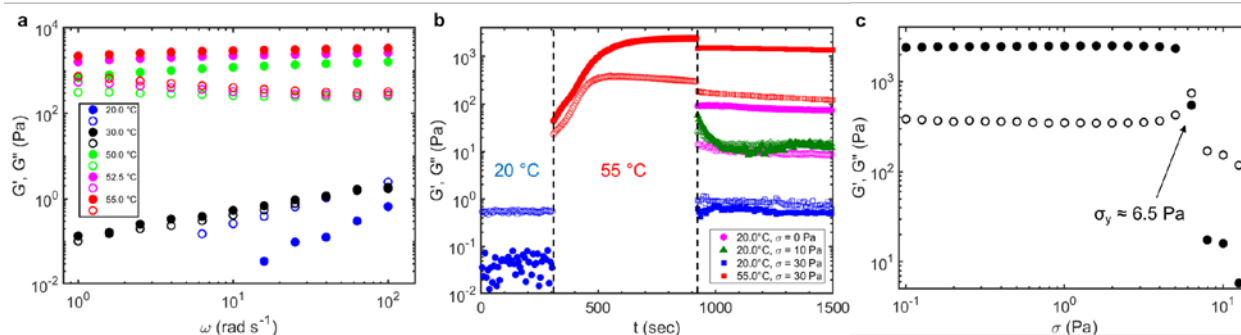


Figure S3. Rheological characterization of the model nanoemulsion system. The nanoemulsion is composed of  $P = 0.33$  and  $\phi = 0.3$  with a droplet diameter  $D = 50$  nm. (a) Linear viscoelasticity,  $G'$  and  $G''$ , as a function of angular frequency,  $\omega$ , at rising temperatures. (b) Reversibility (20-55-20 °C with different shear stresses,  $\sigma$ ) and recovery (20-55-55 °C with  $\sigma$ ) tests. (c) LAOS measurement at 55 °C to determine yield stress,  $\sigma_y \approx 6.5$  Pa. For all figures:  $G'$  = closed symbols and  $G''$  = open symbols.

### S2.3 Effect of total [SDS] on the nanoemulsion gel properties

In our *a priori* estimation of the interactive potentials, the free SDS in the continuous phase contributes to the depletion interaction and the Debye length,  $\kappa$  (Fig. 2c and Fig. 3). Therefore, for the same droplet size, polymer and oil volume fractions, the decrease in the total [SDS] will give rise to a decrease in the depletion interaction and the electrostatic screening, leading to the increase in the gelation temperature and the decrease in the gel strength. To validate these predictions, we studied the effect of the total [SDS] on the gel properties. The results are shown in Figure S4. As expected, the  $T_{\text{gel}}$  increases and  $G_P$  decreases as the less SDS is added.

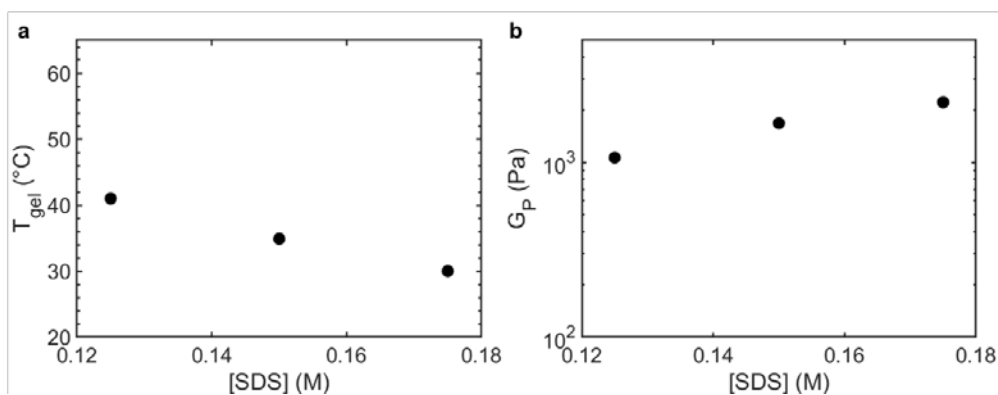


Figure S4. Gelling mechanism as a function of total [SDS] in the nanoemulsion. The PEGMA and oil volume fractions are 0.33 and 0.3 respectively. The droplet diameter is 50 nm. The figure shows (a)  $T_{\text{gel}}$  and (b)  $G_P$  as a function of [SDS].

### S3 Nanoemulsion droplet characterizations

We assumed the colloidal gelation is due to a decrease in electrostatic repulsion via a surfactant displacement mechanism. To validate the hypothesis, we measured the zeta potential of the nanoemulsion droplets (Section S3.1) and investigated how PEGMA replaces SDS (Section S3.2 to S3.4) at rising temperatures. The details of the experiments can be found in Methods section.

#### S3.1 Zeta potential, $\xi$ , of the nanoemulsion droplets

Figure S5 shows the results of  $\xi$  as a function of temperature. As expected,  $\xi$  decreases with temperature (red) in the presence of PEGMA, and the changes in the zeta potential are much larger than measurement error bars, suggesting SDS desorbs from the droplets which leads to the decreases in the electrostatic repulsion (the desorption will be analyzed quantitatively in Section S3.4). On the other hand,  $\xi$  remains unchanged when no PEGMA is added to the system (blue). The observation in Figure S5 supports our gelling mechanism in which the surfactant displacement of the ionic surfactants (SDS) only takes place when the amphiphilic oligomers (PEGMA) are added to the nanoemulsion system.

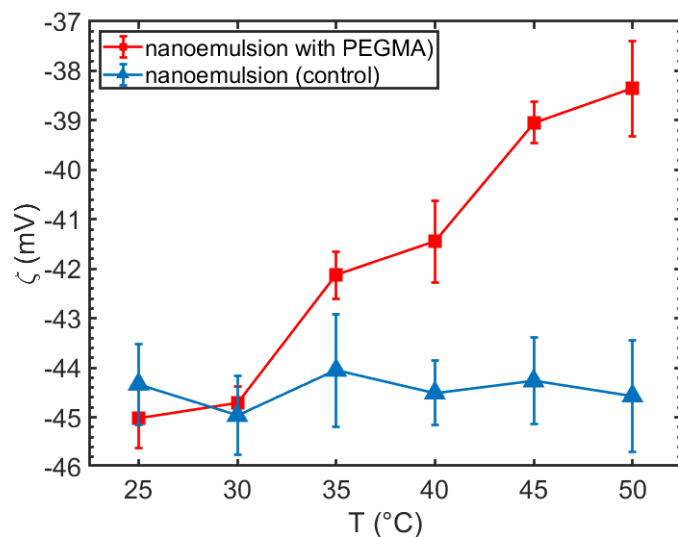


Figure S5. Zeta potential,  $\xi$ , of the nanoemulsion as a function of temperature,  $T$ .  $\xi$  only decreases in the presence of PEGMA, supporting our proposed gelation mechanism where the decrease in electrostatic repulsion results from displacement of the ionic surfactant. Error bars are standard errors from 25-30 independent measurements.

### S3.2 Isothermal titration calorimetry (ITC) experiment

To further probe the surfactant displacement mechanism, ITC was conducted to study the adsorption of PEGMA onto nanoemulsion droplets. As described in the Methods section, the measurements were performed by titrating PEGMA solution into the nanoemulsion (PDMS droplets suspended in an aqueous solution of  $[SDS] = 5.3 \text{ mM}$ ) at various temperatures. The ITC instrument measures the heat associated with the mixing, including the heat of PEGMA adsorption and the heat of PEGMA dilution. The heat of dilution can be measured using a blank test by titrating PEGMA into the SDS solution ( $[SDS] = 5.3 \text{ mM}$ ), which was served as the background signal to correct the raw adsorption data.

Figure S6 shows an example of the result from an ITC measurement (red curve) and the corresponding blank test (blue curve) at  $T = 45.0 \text{ }^\circ\text{C}$ . Note that the result is not yet corrected by the background. The direction of the PEGMA adsorption data suggests the adsorption is an endothermic process, which supports our proposed mechanism (Figure 2a) and rheological data that the gelation and the surfactant displacement take place at elevated temperatures. The data shown in Figure S6 were then analyzed to obtain the detailed adsorption information in Section S3.3.

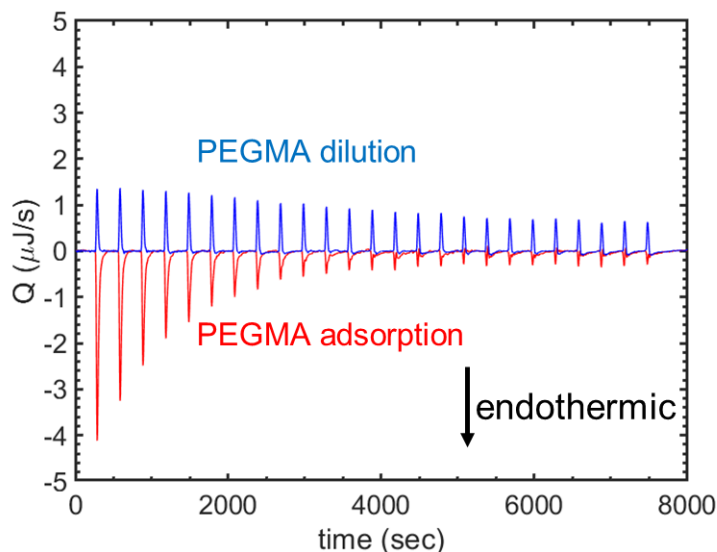


Figure S6. Results of an ITC measurement (red curve) and the corresponding blank test (blue) at  $T = 45.0 \text{ }^\circ\text{C}$ . The direction of the arrow indicates the endothermic process.

### S3.3 ITC Data analysis

To further obtain the quantitative information of PEGMA adsorption behavior, the background-corrected data (Figure S7) were fitted to an independent binding model using the data analysis software NanoAnalyze (TA Instruments). The independent binding model assumes all sites are equal in affinity and independent, and has been widely used in studies of small molecule binding,<sup>7</sup> macromolecule-ligand interactions,<sup>8</sup> adsorption of small molecules onto nanoparticles<sup>9</sup> and even adsorption of proteins onto nanoparticles.<sup>10,11</sup>

To establish the adsorption isotherm from the independent binding model, we performed the equations that have been well-developed and widely-used in the literature.<sup>8,10</sup> First, the binding reaction with an equilibrium constant,  $K_A$ , is considered and shown as followed



where  $NEs$  is the binding site on the nanoemulsion droplet and  $P$  is PEGMA.

The degree of saturation,  $f_A$ , is then defined as

$$f_A = \frac{[NEs \cdot P]}{[NEs] + [NEs \cdot P]} = \frac{K_A[P]}{1 + K_A[P]} \quad (S2)$$

Since all binding sites are assumed to be equal and independent, following relations can be established,

$$[P] = [P]_o - N[NE \cdot P] \quad (S3)$$

$$[NE] = [NE]_o - [NE \cdot P] = [NE]_o(1 - f_A) \quad (S4)$$

where  $N$  is the number of PEGMA adsorbed onto the droplet,  $[P]_o$  is the total concentration of PEGMA and  $[NE]_o$  is the total concentration of the nanoemulsion droplets.

Using Eq. (S2) to (S4),  $f_A$  can be expressed as follows,

$$f_A = \frac{1 + \frac{[P]_o}{N[NE]_o} + \frac{1}{NK_A[NE]_o}}{2} - \frac{1}{2} \sqrt{\left(1 + \frac{[P]_o}{N[NE]_o} + \frac{1}{NK_A[NE]_o}\right)^2 - \frac{4[P]_o}{N[NE]_o}} \quad (S5)$$

The heat measured from the ITC experiment,  $Q$ , is then calculated as,

$$Q = \Delta H V_{cell} N[NE]_o f_A \quad (S6)$$

where  $\Delta H$  is PEGMA adsorption heat and  $V_{cell}$  is volume of sample cell. Therefore,

$$Q = \Delta H V_{cell} N [NE]_o \left[ \frac{1 + \frac{[P]_o}{N[NE]_o} + \frac{1}{NK_A[NE]_o}}{2} - \frac{1}{2} \sqrt{\left( 1 + \frac{[P]_o}{N[NE]_o} + \frac{1}{NK_A[NE]_o} \right)^2 - \frac{4[P]_o}{N[NE]_o}} \right] \quad (S7)$$

Eq. (S7) is the adsorption isotherm associated with the heat and can be used in data analysis. Alternatively, consider the ITC measurement is done by discretely injecting certain amount of PEGMA solution into the nanoemulsion, the change in heat,  $\Delta Q$ , from injections can be expressed as,

$$\Delta Q = Q(i) - Q(i-1) + \frac{V_{inj}}{V_o} \left( \frac{Q(i) + Q(i-1)}{2} \right) \quad (S8)$$

where  $V_{inj}$  is the injection volume each time and  $V_o$  is the initial cell volume.

Figure S7 shows an example of the data analysis at  $T = 45.0$  °C. The data (closed symbols) has been corrected from the blank test and is shown as a function of number of injections. The solid line indicates the result of model fitting using Eq.(S7) and (S8).

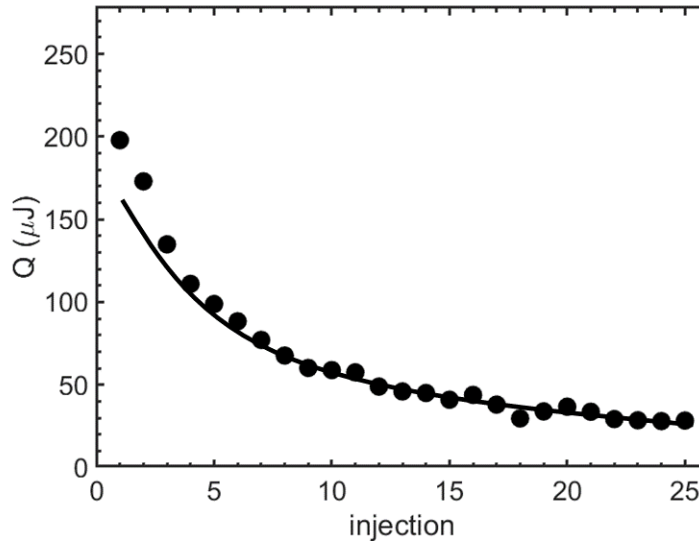


Figure S7. Example of ITC data analysis at  $T = 45.0$  °C. Closed symbols: background-corrected data. Solid line: model fitting using Eq. (S7) and (S8).

Figure S8 concludes the results from ITC measurements at elevated temperatures. Figure S8a shows that the number of PEGMA adsorbed per droplet increases at the elevated temperatures. Along with the zeta potential shown in Figure S5 where the magnitude decreases with T, the results are the direct evidence of the thermally-triggered surfactant displacement mechanism. Moreover, the resulting values in Figure S8a can be further used to estimate the surface potential of nanoemulsion droplets and we show that the resulting values are consistent with the measured zeta potentials in Section S3.4.

Figure S8b shows that the heat of PEGMA adsorption is a function of temperature. First, the result shows the adsorption process is an endothermic reaction across the temperature window, suggesting the entropy of the system increases during the adsorption.<sup>10,12</sup> Such increase in the entropy results from the increase in the translational entropy of the water molecules during the dehydration of the PEGMA hydrophobic groups.<sup>10,12</sup> Therefore, the endothermic behavior supports our proposed mechanism where the dehydration of the hydrophobic groups of the oligomers drives the adsorption. Second, the magnitude of the adsorption heat decreases as the temperature increased. The decreasing heat suggests PEGMA is less stabilized in the continuous phase at elevated temperatures and to validate this hypothesis we compared the blank tests at different temperatures. As shown in Figure S9, as expected, the dilution is an exothermic reaction across the temperature window, and the magnitude of the heat flow decreases at elevated temperatures. The result suggests that PEGMA is more stabilized in the continuous phase at lower temperatures, supporting the observation that less adsorption heat is required at higher temperatures.

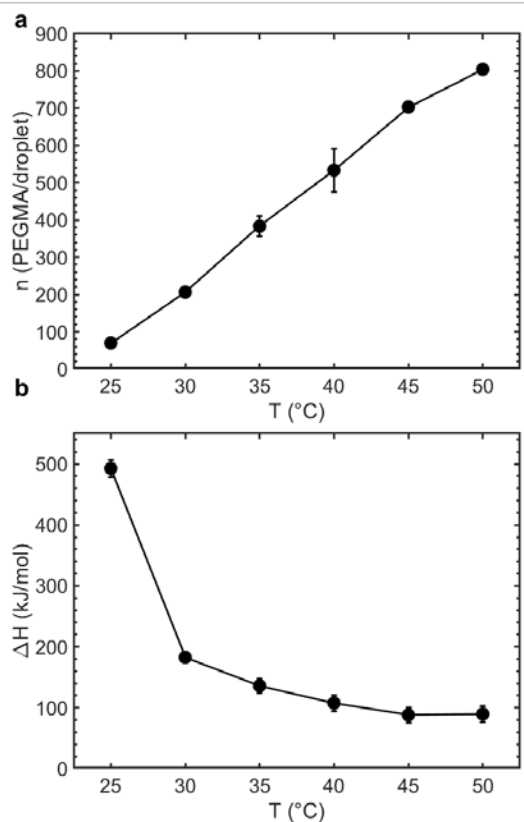


Figure S8. ITC results as a function of temperature. (a) The number of PEGMA adsorbed per droplets,  $n$ . (b) The heat of PEGMA adsorption onto the nanoemulsion droplets,  $\Delta H$ . For both figures, the solid lines are drawn to guide the eye. Error bars are one standard deviation from 3 to 4 independent measurements.

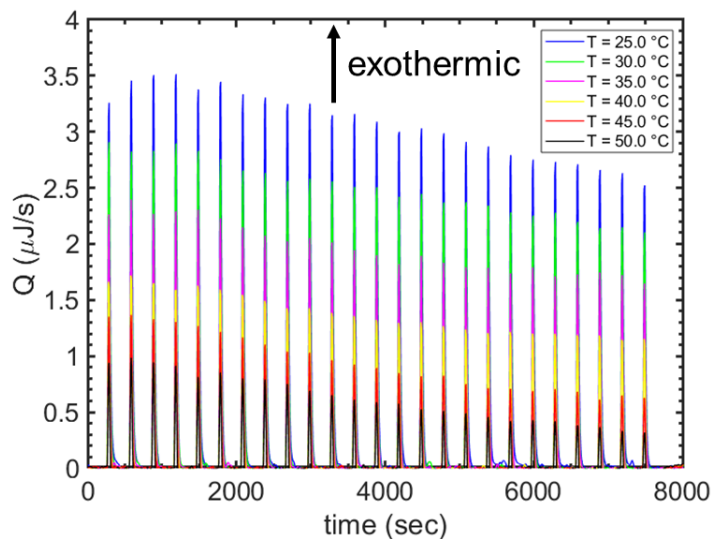


Figure S9. Dilution of PEGMA (blank test) at different temperatures. At higher temperature, PEGMA is less stabilized in the continuous phase as the magnitude of the heat flow,  $Q$ , is smaller.

### S3.4 Estimation of droplet surface electrostatic potential

The PEGMA adsorption shown in Figure S8a allows us to calculate the surface potential,  $\psi_o$ , of nanoemulsion droplets and compare the resulting  $\psi_o$  with measured zeta potentials in Figure S5. To estimate  $\psi_o$ , Grahame equation was used<sup>13</sup>

$$\psi_o = \frac{2kT}{ze} \sin^{-1} \left( \frac{\sigma}{\sqrt{8kTn_\infty \epsilon_o \epsilon_r}} \right) \quad (\text{S9})$$

where  $k$  is Boltzmann constant,  $T$  is the absolute temperature,  $z$  is the valence (charge number),  $\sigma$  is the surface charge density (i.e. surface SDS density since  $z_{SDS} = 1$ ),  $n_\infty$  is the bulk concentration of ions,  $\epsilon_o$  is the permittivity of free space and  $\epsilon_r$  is the relative permittivity of water<sup>14</sup> since the ITC and zeta potential measurements were performed under a diluted condition (Methods).

The Grahame equation has been used to estimate the surface potential of colloids<sup>15</sup> by considering the surface charge density,  $\sigma$ , estimated as

$$\sigma = \frac{(n_{SDS} - xn_{PEGMA})e}{A} \quad (\text{S10})$$

where  $n_{SDS}$  is number of SDS on a droplet and is estimated by considering the area of SDS occupied on the oil droplet ( $= 0.617 \text{ nm}^2/\text{molecule}$ <sup>16</sup>),  $n_{PEGMA}$  is the number of PEGMA adsorbed onto droplet from ITC measurements,  $A$  is the surface area of a droplet and  $x$  is the number of SDS replaced by PEGMA, which is not necessarily equal to unity as will be discussed shortly. To simplify the calculation, here we assume the number of replaced SDS molecules is the same across the temperature window, i.e.  $x$  is assumed to be a constant and independent of temperature.

By using Eq. (S9), (S10) and the values listed in Figure S8a, the resulting estimated surface potentials at elevated temperatures are shown in Figure S10b. Figure S10a lists the temperature-dependent zeta potentials from Figure S5 for comparison. Again, the magnitude of the measured  $\xi$  decreases (less negative) with temperature, suggesting the desorption of SDS, and the trend of  $\xi$  should also reflect the behavior of the surface potential,<sup>17-19</sup> i.e. the magnitude of  $\psi_o$  should also decrease with temperature. Interestingly, as shown in Figure S10b, the  $|\psi_o|$  increases with temperature for  $x = 1$  and 2. Such counter-intuitive observation is possible since  $\epsilon_r$  (See Table 1)

is temperature-dependent<sup>14</sup> (as well as  $T$ ). The trend of  $\psi_o$  starts to follow the trend of  $\xi$  as  $x \geq 3$ , indicating at least three SDS molecules are replaced by one PEGMA under the adsorption process.

Based on Eq. (S9) and (S10), a decreasing  $|\psi_o|$  at elevated temperatures can be always obtained when  $x \geq 3$ , although the value of  $x$  should be finite. To determine a reasonable range of  $x$ , we considered the adsorption heat,  $\Delta H$ , associated with the surfactant displacement process.

According to the proposed mechanism shown in Figure 2a, PEGMA adsorption in fact includes two steps: SDS desorption and PEGMA adsorption, and the heat associated with these two steps are lumped into a single  $\Delta H$  in the ITC data analysis. According to prior work which studied SDS adsorption/desorption thermodynamics at the oil/water interface,<sup>20-22</sup> the desorption heat of SDS is  $\approx 15$ -20 kJ/mole (endothermic process). Along with the ITC results listed in Figure S8b where  $\Delta H$  is  $\approx 100$  kJ/mole, a reasonable range of  $x$  is 3 to 5 here.

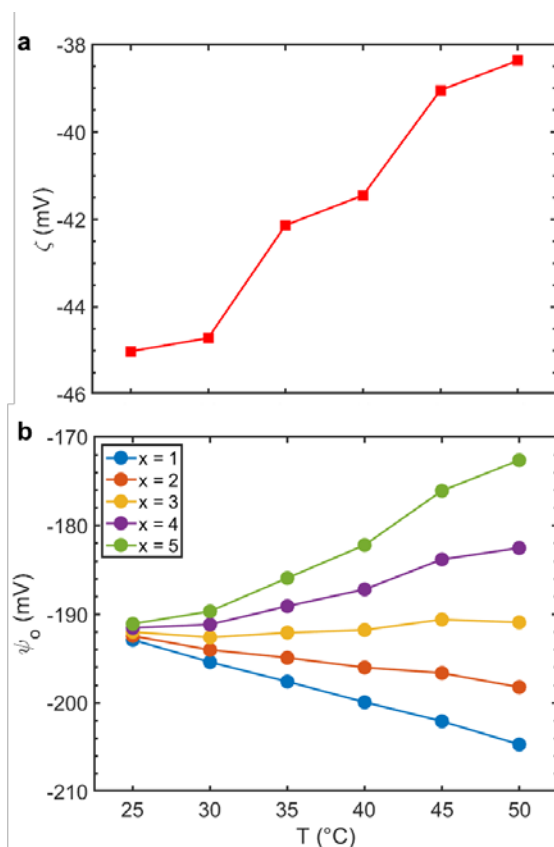


Figure S10. Comparison of the measured zeta potential,  $\xi$ , and the estimated surface potential,  $\psi_o$ , of the nanoemulsion droplets. (a) Measured  $\xi$  from Figure S5. (b) Estimated  $\psi_o$  using Eq. (S9), (S10) and the values listed in Figure S8a. The solid lines are drawn to guide the eye.

## References

- (1) Gupta, A.; Eral, H. B.; Hatton, T. A.; Doyle, P. S. Nanoemulsions: formation, properties and applications. *Soft Matter* **2016**, *12*, 2826–2841.
- (2) Mason, T. G.; Wilking, J. N.; Meleson, K.; Chang, C. B.; Graves, S. M. Nanoemulsions: formation, structure, and physical properties. *J. Phys. Condens. Matter* **2006**, *18*, R635–R666.
- (3) Chambon, F.; Winter, H. H. Linear Viscoelasticity at the Gel Point of a Crosslinking PDMS with Imbalanced Stoichiometry. *J. Rheol.* **1987**, *31*, 683–697.
- (4) Winter, H. H.; Chambon, F. Analysis of Linear Viscoelasticity of a Crosslinking Polymer at the Gel Point. *J. Rheol.* **1986**, *30*, 367–382.
- (5) Cheng, L.-C.; Godfrin, P. D.; Swan, J. W.; Doyle, P. S. Thermal processing of thermogelling nanoemulsions as a route to tune material properties. *Soft Matter* **2018**, *14*, 5604–5614.
- (6) Cipelletti, L.; Ramos, L. Slow dynamics in glasses, gels and foams. *Curr. Opin. Colloid Interface Sci.* **2002**, *7*, 228–234.
- (7) Pons Siepermann, C. A.; Myerson, A. S. Inhibition of Nucleation Using a Dilute, Weakly Hydrogen-Bonding Molecular Additive. *Cryst. Growth Des.* **2018**, *18*, 3584–3595.
- (8) Martinez, J. C.; Murciano-Calles, J.; S., E.; Iglesias-Bexiga, M.; Luque, I.; Ruiz-Sanz, J. Isothermal Titration Calorimetry: Thermodynamic Analysis of the Binding Thermograms of Molecular Recognition Events by Using Equilibrium Models. In *Applications of Calorimetry in a Wide Context - Differential Scanning Calorimetry, Isothermal Titration Calorimetry and Microcalorimetry*; InTech, 2013.
- (9) Joshi, H.; Shirude, P. S.; Bansal, V.; Ganesh, K. N.; Sastry, M. Isothermal titration calorimetry studies on the binding of amino acids to gold nanoparticles. *J. Phys. Chem. B* **2004**, *108*, 11535–11540.
- (10) Lindman, S.; Lynch, I.; Thulin, E.; Nilsson, H.; Dawson, K. A.; Linse, S. Systematic Investigation of the Thermodynamics of HSA Adsorption to N-tert-Butylacrylamide

- Copolymer Nanoparticles . Effects of Particle Size and Hydrophobicity. *Nano Lett.* **2007**, 7, 914–920.
- (11) Welsch, N.; Lu, Y.; Dzubiella, J.; Ballauff, M. Adsorption of proteins to functional polymeric nanoparticles. *Polymer* **2013**, 54, 2835–2849.
- (12) Saha, P.; Chowdhury, S. Insight Into Adsorption Thermodynamics. In *Thermodynamics; IntechOpen*, 2011.
- (13) Hiemenz, P. C.; Rajagopalan, R. Principles of Colloid and Surface Chemistry; *CRC Press*, **1997**.
- (14) Malmberg, C. G.; Maryott, A. A. Dielectric constant of water from 0 to 100 C. *J. Res. Natl. Bur. Stand.* **1956**, 56, 1.
- (15) Zeng, Y.; Grandner, S.; Oliveira, C. L. P.; Thünemann, A. F.; Paris, O.; Pedersen, J. S.; Klapp, S. H. L.; Von Klitzing, R. Effect of particle size and Debye length on order parameters of colloidal silica suspensions under confinement. *Soft Matter* **2011**, 7, 10899–10909.
- (16) Kanellopoulos, A. G.; Owen, M. J. Adsorption of sodium dodecyl sulphate at the silicone fluid/water interface. *Trans. Faraday Soc.* **1971**, 67, 3127–3138.
- (17) Attard, P.; Antelmi, D.; Larson, I. Comparison of the zeta potential with the diffuse layer potential from charge titration. *Langmuir* **2000**, 16, 1542–1552.
- (18) Sprycha, R. Electrical double layer at alumina/electrolyte interface. I. Surface charge and zeta potential. *J. Colloid Interface Sci.* **1989**, 127, 1–11.
- (19) Rabinovich-Guilatt, L.; Couvreur, P.; Lambert, G.; Goldstein, D.; Benita, S.; Dubernet, C. Extensive surface studies help to analyse zeta potential data: The case of cationic emulsions. *Chem. Phys. Lipids* **2004**, 131, 1–13.
- (20) Gillap, W. R.; Weiner, N. D.; Gibaldi, M. Ideal behavior of sodium alkyl sulfates at various interfaces. Thermodynamics of adsorption at the oil-water interface. *J. Phys. Chem.* **1968**, 72, 2222–2227.
- (21) Moreno, M. J.; Bastos, M.; Velazquez-Campoy, A. Partition of amphiphilic molecules to

lipid bilayers by isothermal titration calorimetry. *Anal. Biochem.* **2010**, 399, 44–47.

- (22) Tan, A.; Ziegler, A.; Steinbauer, B.; Seelig, J. Thermodynamics of sodium dodecyl sulfate partitioning into lipid membranes. *Biophys. J.* **2002**, 83, 1547–1556.